

LETTERS

Crossover from 'mesoscopic' to 'universal' phase for electron transmission in quantum dots

M. Avinun-Kalish¹, M. Heiblum¹, O. Zarchin¹, D. Mahalu¹ & V. Umansky¹

The measurement of phase in coherent electron systems—that is, 'mesoscopic' systems such as quantum dots—can yield information about fundamental transport properties that is not readily apparent from conductance measurements. Phase measurements on relatively large quantum dots¹ recently revealed that the phase evolution for electrons traversing the dots exhibits a 'universal' behaviour, independent of dot size, shape, and electron occupancy^{2,3}. Specifically, for quantum dots in the Coulomb blockade regime, the transmission phase increases monotonically by π throughout each conductance peak; in the conductance valleys, the phase returns sharply to its starting value. The expected mesoscopic features in the phase evolution—related to the dot's shape, spin degeneracy or to exchange effects—have not been observed, and there is at present no satisfactory explanation for the observed universality in phase behaviour⁴. Here we report the results of phase measurements on a series of small quantum dots, having occupancies of between only 1–20 electrons, where the phase behaviour for electron transmission should in principle be easier to interpret. In contrast to the universal behaviour observed thus far only in the larger dots, we see clear mesoscopic features in the phase measurements when the dot occupancy is less than ~ 10 electrons. As the occupancy increases, the manner of phase evolution changes and universal behaviour is recovered for some 14 electrons or more. The identification of a transition from the expected mesoscopic behaviour to universal phase evolution should help to direct and constrain theoretical models for the latter.

The experimental configuration is shown in Fig. 1. The interferometer, formed in a two-dimensional electron gas (a GaAs-AlGaAs heterostructure), consists of emitter E and collector C constrictions, each formed by a quantum point contact (QPC), and a few base regions B in between. The grounded base regions (chemical potential $\mu_B = 0$) serve as draining reservoirs, ensuring that interference is only between two paths⁵. A centre island separates the incoming electrons into two paths and embedded within it is the plunger gate of the quantum dot, which controls the occupancy of the dot. The transmission phase of the quantum dot adds to the phase gain in the left arm and is then compared with the phase of the right arm. Threading a weak magnetic field through the area of the interferometer adds an Aharonov–Bohm (AB) phase to one arm, $\Delta\phi_{AB} = 2\pi \Phi/\Phi_0$, where Φ is the magnetic flux enclosed by the two arms and $\Phi_0 = h/e$ is the flux quantum^{6,7}. A QPC is coupled capacitively to the quantum dot, hence sensing its potential—enabling counting of the electrons in the dot^{8,9}.

A simplified model of the quantum dot is a resonant tunnelling device: a potential well confined between two tunnelling barriers with quasi-bound resonant states, E_n . The transmission amplitude exhibits maxima whenever the Fermi energy in the leads, E_F , coincides with E_n . Owing to the finite coupling between well and leads, the levels are broadened to Γ_n (dwell time $\sim h/\Gamma_n$), with the

transmission through the quantum dot, t_{QD} , described by the Breit–Wigner expression¹⁰ $t_{QD} = C_n(i\Gamma/2)/(E_F - E_n + i\Gamma/2)$. Here, the C_n s are positive or negative real numbers (since at a zero magnetic field the hamiltonian is real), depending on the parity of the n th wavefunction with respect to the 'in' and 'out' openings of the quantum dot. The phase of the transmission amplitude evolves by

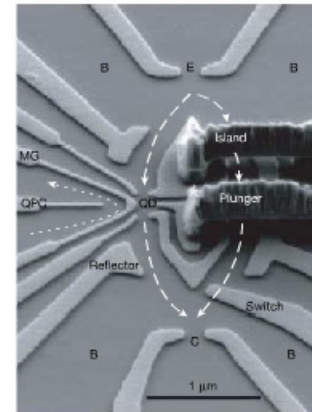


Figure 1 | SEM micrograph of the device. The two-path interferometer consists of a patterned high mobility two-dimensional electron gas formed ~ 53 nm below the surface of a GaAs–AlGaAs heterostructure, with areal carrier density $n_s = 3.3 \times 10^{11} \text{ cm}^{-2}$ and mobility $\mu = 1.6 \times 10^6 \text{ cm}^2 \text{ V}^{-1} \text{ s}^{-1}$ at $T = 4.2$ K, resulting in an elastic mean free path $l = 14.5 \mu\text{m}$. To ensure only two interfering paths from emitter E to collector C, the reflected and scattered paths are collected by the base B regions through openings formed between the gates of the reflectors and the quantum point contacts (QPCs). The 'switch' gate turns off the right path to allow tuning of the quantum dot (QD). The quantum dot is composed of two QPCs and a middle gate (MG) in between, allowing formation of 'small' and 'large' dots. The 'plunger' gate is embedded in the centre island, and is connected via a metallic air bridge to the outside in order to allow biasing without crossing the right (reference) arm of the interferometer. Similarly, another bridge biases the centre island. The magnetic flux is contained in the area between the two paths (shown by the dashed lines). The QPC counting detector, separated from the quantum dot by MG, has its own current path (shown by the dotted line). The transmission from E to C oscillates with the AB flux with phase dependent on the transmission phase of the quantum dot.

¹Braun Center for Submicron Research, Department of Condensed Matter Physics, Weizmann Institute of Science, Rehovot 76100, Israel.

π through each resonance, while the relative phase between adjacent resonances, determined by C_{ex} , can be 0 or π (ref. 11). However, in contrast, all previous measurements, conducted with relatively large occupancy quantum dots, consistently led only to positive C_{ex} s (refs 2, 3, and our unpublished data).

A large number of theoretical publications have been devoted to the puzzle of phase evolution (see recent summary⁴). They may be grouped in three main classes. The first class questions whether the measured phase is the 'intrinsic transmission phase' of the quantum dot or a modified phase due to multiple paths traversing the interferometer^{12,11}. The second class considers transport that is mediated by interplay of more than one quantum state. A common scenario assumes an existence of a dominant level strongly coupled to the leads, responsible for shuttling the electrons^{14,15}. After occupation the electron is unloaded to a localized level, weakly coupled to the leads, allowing the dominant level to be free again to transfer another electron. Hence, the observed phase is only that of the dominant level. Based on this idea other models examined only two levels, with one of the levels dominant, adding spins, adding interactions, or assuming a finite temperature¹⁶⁻¹⁸. Interaction between two levels was invoked also in a quantum dot where the plunger gate couples

with different strengths to different energy states, leading thus to avoided level crossing and charge shuttling between levels⁴. The third class deals with specific energies where both the imaginary and the real parts of the transmission coefficient vanish⁹. These singular points, which explain the phase slips in the valleys, might result from a deviation from a strictly zero-dimensional system¹ or from the existence of Fano resonances in the dot²⁰, but they can not explain the 'in phase' behaviour of all peaks. Naturally, one would expect the breakdown of every model for some tuning parameters, which we, thus far, have never observed. Still, some models may predict an 'in phase' behaviour for a very large sequence of peaks but not universal behaviour. We return to this issue later.

At low enough temperatures, both the phase coherence length and the elastic mean free path exceed the sample size. The current in a grounded collector is $I_{\text{EC}} = (2e^2/h)T_{\text{EC}}V_{\text{ED}}$, where V_{ED} is the voltage applied between emitter and base, and T_{EC} is the transmission probability from emitter to collector²¹. The transmission T_{EC} results from a coherent sum of the two trajectory amplitudes that traverse the two arms of the interferometer, $|t_{\text{EC}}|^2 = T_{\text{EC}}$, and $t_{\text{EC}} = t_{\text{L}} + t_{\text{R}}$, where $t_{\text{L,R}}$ is the transmission amplitude associated with the left and right paths, respectively. The phase dependent part is $T_{\text{EC}} \propto |t_{\text{L}}||t_{\text{R}}|\cos[\Delta\varphi_{\text{AB}} + \varphi(t_{\text{R}}) - \varphi(t_{\text{L}})]$ with $\varphi(t_{\text{L,R}})$ the corresponding phases, and $\varphi(t_{\text{L}}) = \varphi_0(t_{\text{L}}) + \varphi_{\text{QD}}$ the accumulated phase in the left arm. Hence, T_{EC} oscillates as a function of magnetic flux with period Φ_0 , with any change in φ_{QD} leading to a similar change in the phase of the oscillating collector current.

Measurements were done in a dilution refrigerator ($T_{\text{lattice}} \approx 20$ mK, $T_{\text{detector}} = 30$ mK) with an a.c. excitation voltage $V_{\text{ED}} = 2-20 \mu\text{V}$

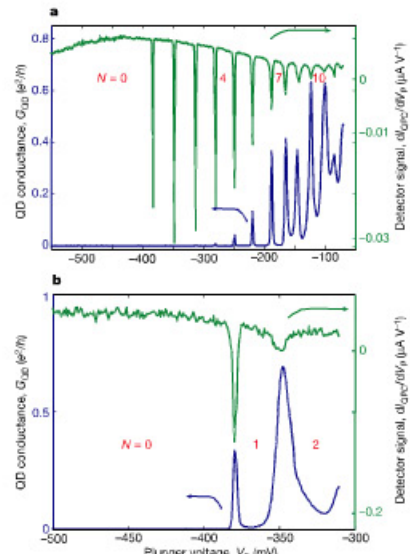


Figure 2 | Electron counting in the quantum dot by a QPC detector. In the Coulomb blockade regime we expect V_{QD} to increase as the plunger gate voltage V_{p} increases, eventually reaching $V_{\text{QD}} = (e/2C_{\text{QD}}) + \Delta E/e$, with C_{QD} the self capacitance of the dot and $e/2C_{\text{QD}}$ the charging energy of the dot. At this potential, an electron enters the quantum dot and screens the positive potential induced by the plunger, resulting in a potential drop. Hence, the quantum dot potential, and consequently the conductance of the QPC counting detector, exhibit a saw-tooth-like behaviour. The derivative $dI_{\text{QPC}}/dV_{\text{p}}$ is a series of negative dips. **a**, Conductance peaks of the quantum dot (blue) and the corresponding detector dips (green). The detector proves the presence of electrons, even though the quantum dot conductance is too small to be measured. **b**, The quantum dot is retuned by opening the 'in' and 'out' QPCs, and changing the voltage on MG in order to allow measurable conductance of the first few electrons.

530

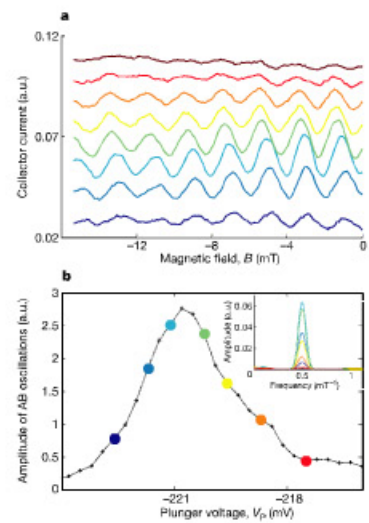


Figure 3 | Phase measurement procedure. **a**, The quantum dot is first tuned to conduct, and the AB oscillations (with V_{p} as a parameter) are monitored throughout a conductance peak at the chosen values shown in **b**. Note the change in amplitude and in phase among the different traces (that are shifted vertically for clarity). **b**, The amplitude of the oscillations plotted as a function of V_{p} (the coloured points correspond to the coloured traces in **a**). The amplitude was determined by a fast Fourier transform. Inset, Fourier transforms of the oscillations indicating a single AB period corresponding to an addition of a flux quantum h/e to the area enclosed by the two paths.

(frequency ~ 23 Hz). The integrity of the 'two-path' interferometer was verified by observing a single period $\Delta\phi = \phi_0 = h/e$ in the interference signal (see below), indicating only two-path interference. Higher orders, with period ϕ_0/n , were at least four orders of magnitude smaller. The quantum dot was formed by adjusting the resistance of its 'in' and 'out' QPCs to be greater than $h/2e^2$, namely, in the Coulomb blockade regime. To ensure transport mainly through one level we tuned the dot to $T < \Delta E$, with $\Delta E \approx 0.5$ meV and $T = 30\text{--}300$ μeV , with the temperature being the smallest energy, $k_B T < 3$ μeV . In the 'constant interaction' model, the complex interaction among the electrons is represented by a capacitor C_{QD} , leading to a charging energy $U = e^2 C_{\text{QD}}^{-1} \approx 1\text{--}3$ meV. Varying the plunger gate voltage V_p changes the potential landscape in the quantum dot and consequently the occupation, N . Classically, for a certain V_p degeneracy takes place, $E(N) = E(N+1)$; allowing the number of electrons to fluctuate between N and $N+1$ with no energy cost, allowing current flow.

The electron counting detector is a separately biased QPC, capacitively coupled to the quantum dot^{4,9}. The induced potential in the QPC is $V_{\text{QPC}} = V_{\text{QD}} C_{\text{QPC-QD}}/C_{\text{QPC}}$, where C_{QPC} is the self capacitance of the QPC and $C_{\text{QPC-QD}}$ is the mutual capacitance between quantum dot and QPC detector. Charging the quantum dot affects V_{QPC} and the conductance of the QPC, which in turn is analysed by a small current (20–80 nA). The potential energy of the quantum dot rises linearly with plunger voltage, reaching eventually $\Delta E + e^2/2C_{\text{QD}}$, followed by a sharp drop when an electron enters the

dot. Indeed, the conductance of the QPC detector exhibited repetitive saw-tooth-like oscillations as a function of V_p , with one period for every additional electron entering the dot. We measured the derivative dI_{QPC}/dV_p (via applying a small a.c. voltage to the plunger gate), resulting in easily identifiable dips in the derivative (see Fig. 2). Note that determining the occupancy of the quantum dot via a separate detector is necessary since for sufficiently negative V_p the quantum dot inadvertently pinches off (via the mutual coupling among the different gates). Consequently, the dot's conductance peaks weaken and are impossible to resolve. As seen in Fig. 2a, the conductance dips of the detector persisted down to $V_p \approx -400$ mV, much beyond $V_p \approx -300$ mV where the conductance peaks of the quantum dot were too small to resolve. We carefully retuned the quantum dot without changing its occupancy, in order to maximize the conductance peaks, allowing reliable phase measurements (for example, Fig. 2b).

Varying the magnetic field in a range 0–30 mT, after the quantum dot was tuned to conduct, resulted in relatively high visibility AB oscillations with a single period $\Delta B = \phi_0/\text{area} \approx 2$ mT (see Fig. 3; in a different structure $\Delta B \approx 3.5$ mT). The coherent part of the transmission (Fig. 3b) and the transmission phase (Figs 4–6) were both determined from data such as shown in Fig. 3a by performing a fast complex Fourier transform of the AB oscillations as a function of V_p .

We studied two different configurations of interferometers and quantum dots, as well as thermally recycled structures (which behave as different devices after thermal recycling). A single tuning allowed the addition of only 2–3 electrons without changing drastically the coupling of the dot to the leads or the symmetry of the interferometer. Hence, the quantum dot and the interferometer were

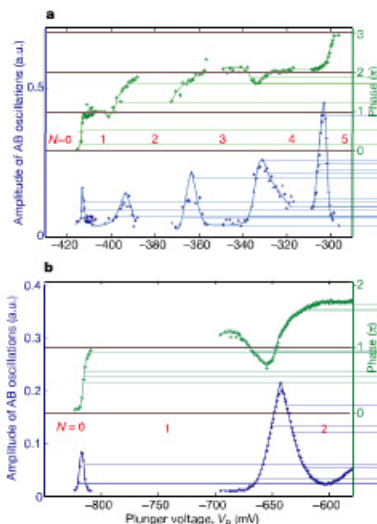


Figure 4 | Phase evolution and coherent conductance for the first few electrons in the quantum dot. The dotted lines are a guide to the eye. **a**, Typical behaviour of the 'amplitude of AB oscillations' and the phase for the first five electrons ($N = 1 \dots 5$). Whereas the first two electrons enter different orbital states, the following two share the same orbital parity with the second electron. **b**, Detailed behaviour of the phase for the first two electrons in a different device. Note the two-orbital singlet, which is robust for all tuning parameters. Before the entry of the second electron, the phase always exhibits a drop—as large as $\pi/2$ —independent of how much the quantum dot is being pinched. It may be related to an onset of Kondo correlation.

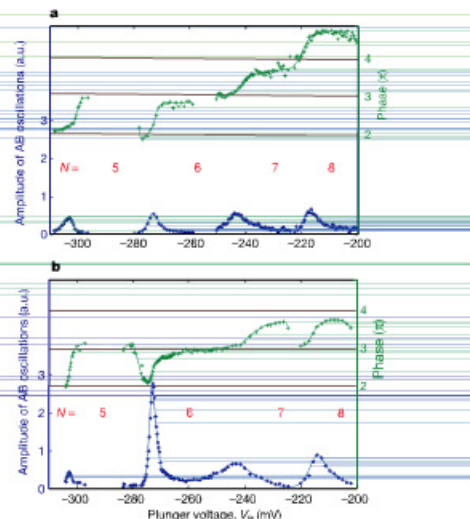


Figure 5 | Two examples of phase evolution for $N = 5\text{--}8$ with different tuning parameters of the quantum dot and the interferometer. This is to demonstrate that the features are mesoscopic, that is, sensitive to the dot's configuration. Whereas the fifth and sixth electrons remain in similar parity states for the two tunings, the seventh and eighth electrons are in different parity orbital states in **a** and in similar parity orbital states in **b**.

returned after every few added electrons, keeping the occupation checked with the QPC detector, in order to optimize the visibility and CB conditions. The measured phase in different occupation regimes was then patched together in order to obtain a continuous phase evolution over a wide range of electron occupation. We present in Figs 4–6 examples of phase and amplitude of the coherent part of the transmission coefficient for an increasing electron number in the quantum dot. We did not subtract any extraneous phase that may be induced in the arms of the interferometer by the varied plunger voltage since this phase is difficult to determine accurately. However, we estimated it to be a weak function of V_p and quite small for the addition of 2–3 electrons at a time.

The phase evolution across the first two conductance peaks and valleys (the first two electrons entering the dot) already exhibited a marked deviation from universal behaviour. As demonstrated in the results of two different dot and interferometer designs, the phase climbed by π for each of the first two added electrons (Fig. 4). Moreover, this dependence was robust and independent of a dot's tunings. Evidently, the different phase of the first two conductance peaks suggests that the first two electrons occupy two opposite parity orbital states, and not one state as assumed thus far^{23–24}. Since the ground state of a two-electron system must be a singlet²⁵, two opposite spins occupy the lowest two states. This is not surprising, since our dots are likely to have a very shallow potential well, and hence a relatively small single particle level spacing, favouring an occupation of two levels in order to minimize the Coulomb repulsion²⁶. We will not speculate here on the reproducible dip in the phase before the entering of the second electron, which is as large as $\pi/2$ (Fig. 4b). Adding the third and fourth electrons (Fig. 4a), the phase evolves from π to 2π —a similar range to the second electron. Consequently, these data suggest that the second to the fourth electrons all occupy similar parity orbital levels. Similarly, the fifth electron evolves from $\sim 2\pi$ to $\sim 3\pi$, which is indistinguishable from a phase evolving from 0 to π of the first electron.

Figure 5a and b shows the sensitivity of the phase to the tuning parameters. While the phase in the fifth, sixth and seventh conductance peaks is independent of tuning parameters, the phase of the eighth electron depends on the tuning parameters. For somewhat different parameters of the quantum dot, the eighth electron has a different parity from that of the seventh electron. The above described examples (Figs 4 and 5) clearly demonstrate a reasonable phase behaviour, sensitive to details of the potential, by showing spin degeneracy, exchange interaction, or Cooper channel interaction²⁶.

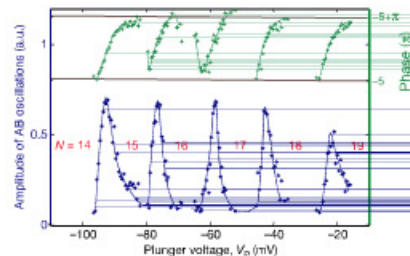


Figure 6 | The quantum dot undergoes universal phase evolution after fourteen electrons have entered. This behaviour is independent of tuning and is ubiquitous to all measured many-electron dots. Note that the absolute value of phase (with respect to the phase of the first electron) is difficult to determine accurately owing to an accumulated phase in the leads or a distortion of the interferometer, so only its approximate value is noted; however, the phase span is always π .

532

This is distinctly different from the repetitive, universal-like, phase rigidity observed in many electron dots²³.

With the addition of more electrons the phase evolves through a transition region, which resembles universal behaviour (not shown). The phase climbs throughout each conductance peak and drops in the valleys, riding though on a rising background phase. However, for dot occupation of some 14 electrons and higher (Fig. 6), the phase 'locks' into the universal behaviour—being then insensitive to the dot's tuning. In other words, the intricacies of shape-dependent level occupation and parity effects disappear altogether.

Since our aim was to explore the validity of the bizarre phase evolution over a large range of parameters, we may now ask: what have we learnt from this new set of measurements? First, that there are two distinct regimes of phase evolution. (1) For occupation 1 to about 10, the phase evolution is highly sensitive to the dot's configuration and occupation. (2) For occupation higher than about 14, phase evolution is universal-like, with phase ranging only between 0 and π , and is independent of the dot's configuration and occupation. Whereas regime (1) can be explained by current understanding of quantum dots, regime (2) presents difficulties, especially since screening is expected to be more effective at higher occupations (possibly leading to single-particle-like behaviour). However, the absence of phase universality in regime (1) is gratifying for two main reasons: first, it confirms that our measured phase is indeed the intrinsic phase of the quantum dot. Otherwise, we would not observe such distinct differences between dilute and highly populated dots. Second, we can now comment on some aspects of the existing theories. An outstanding feature of larger quantum dots is the smaller level spacing, which might lead to levels overlapping. This will favour models that invoke transmission mediated through more than one quantum state.

An illuminating example can be that of a dominant orbital state strongly coupled to the leads. Such a level can be simply a solution of Schrödinger's equation¹⁵, or alternatively, the higher of any two sequential levels. The higher level is broader, since it experiences a lower potential barrier to the leads (Y. Oreg, personal communication). Consequently, a broader level is likely to be occupied, and hence responsible for electron shuttling and the similar phase of many peaks. Still, a theory has to be developed that explains the robustness of the effect for an extremely large number of conductance peaks.

Received 25 February; accepted 8 June 2005.

1. Van Houten, H., Beenakker, C. W. J. & Staring, A. A. W. in *Single Charge Tunneling - Coulomb Blockade Phenomena in Nanostructures* (eds Grabert, H. & Devoret, M. H.) 167–216 (Plenum, New York, 1992).
2. Schuster, R. et al. Phase measurement in a quantum dot via a double slit interference experiment. *Nature* **385**, 417–420 (1997).
3. Ji, Y., Heiblum, M., Sprinzak, D., Mahalu, D. & Shtrikman, H. Phase evolution in a Kondo-correlated system. *Science* **290**, 779–783 (2000).
4. Hackenbroich, G. Phase coherent transmission through interacting mesoscopic systems. *Phys. Rev.* **343**, 463–528 (2000).
5. Yacoby, A., Schuster, R. & Heiblum, M. Phase rigidity and $h/2e$ oscillations in a single-ring Aharonov-Bohm experiment. *Phys. Rev.* **6** 53, 9583–9586 (1996).
6. Aronov, A. G. & Sharvin, Yu. V. Magnetic flux effects in disordered conductors. *Rev. Mod. Phys.* **59**, 755–779 (1987).
7. Aharonov, Y. & Bohm, D. Significance of electromagnetic potentials in the quantum theory. *Phys. Rev.* **115**, 485–491 (1959).
8. Field, M. et al. Measurements of Coulomb blockade with a noninvasive voltage probe. *Phys. Rev. Lett.* **70**, 1311–1314 (1993).
9. Sprinzak, D., Ji, Y., Heiblum, M., Mahalu, D. & Shtrikman, H. Charge distribution in a Kondo correlated quantum dot. *Phys. Rev. Lett.* **88**, 176805 (2002).
10. Breit, G. & Wigner, E. Capture of slow neutrons. *Phys. Rev.* **49**, 519–531 (1936).
11. Hackenbroich, G. & Weidenmüller, H. A. Transmission through a quantum dot in an Aharonov-Bohm ring. *Phys. Rev. Lett.* **76**, 110–113 (1996).
12. Weidenmüller, H. A. Transmission phase of an isolated CB resonance. *Phys. Rev.* **6** 65, 245322 (2000).
13. Aharonov, A., Entin-Wohlman, O., Halperin, B. I. & Imry, Y. Phase measurement in the mesoscopic AB interferometer. *Phys. Rev.* **6** 66, 115311 (2002).
14. Levy Yeyati, A. & Büttiker, M. Scattering phases in quantum dots: An analysis based on lattice models. *Phys. Rev.* **6** 62, 7307–7315 (2000).

15. Silvestrov, P. G. & Imry, Y. Towards an explanation of the mesoscopic double-slit experiment: A new model for charging of a quantum dot. *Phys. Rev. Lett.* **85**, 2565–2568 (2000).

16. Silvestrov, P. G. & Imry, Y. Spin effects and transport in QD with overlapping resonances. *Phys. Rev. B* **65**, 035309 (2002).

17. Silva, A., Oreg, Y. & Gefen, Y. The signs of QD lead matrix elements: The effect on transport vs. spectral properties. *Phys. Rev. B* **66**, 195316 (2002).

18. Oreg, Y. & Gefen, Y. Electron scattering through a quantum dot: A phase lapse mechanism. *Phys. Rev. B* **55**, 13726–13729 (1997).

19. Lee, H. W. Generic transmission zeros and in-phase resonances in time-reversal symmetric single channel transport. *Phys. Rev. Lett.* **82**, 2358–2361 (1999).

20. Entin-Wohlman, O., Aharony, A., Imry, Y. & Levinson, Y. The Fano effect in AB interferometers. *J. Low Temp. Phys.* **126**, 1251–1273 (2002).

21. Büttiker, M. 4-Terminal phase-coherent conductance. *Phys. Rev. Lett.* **57**, 1761–1764 (1986).

22. Kouwenhoven, L. P., Oosterkamp, T. H., Tarucha, S., Austing, D. G. & Honda, H. Coulomb oscillations in few-electron quantum dot. *Physica B* **249–251**, 191–196 (1998).

23. Zumbuhl, D. M., Marcus, C. M., Hanson, M. P. & Gossard, A. C. Voltage-

tunable singlet-triplet transition in lateral quantum dots. *Phys. Rev. B* **66**, 035320 (2002).

24. Kyriakidis, J., Floro-Ladriere, M., Gorga, M., Sachrajda, A. S. & Hawrylak, P. Tunneling spectroscopy in few electron QDs. *Phys. Rev. Lett.* **93**, 256801 (2004).

25. Ashcroft, N. W. & Mermin, N. D. *Solid State Physics* Ch. 32 (Holt, Rinehart and Winston, Orlando, 1976).

26. Oreg, Y., Brouwer, P. W., Waintal, X. & Halperin, B. I. In *Nano-Physics and Bio-Electronics* (eds Chakraborty, T., Peeters, F. & Sivan, U.) Ch. 5 (Elsevier, Amsterdam, 2002).

Acknowledgements The work was partly supported by the Minerva foundation, the German Israeli Project Cooperation (DIP), the German Israeli Foundation (GIF), and the QUACS network. We are grateful to Y. Levinson, Y. Oreg and A. Yacoby for discussions. We thank M. Popadic for collaboration in the experiments.

Author Information Reprints and permissions information is available at npg.nature.com/reprintsandpermissions. The authors declare no competing financial interests. Correspondence and requests for materials should be addressed to M.H. (heilblum@wisemail.weizmann.ac.il).